Nano Energy 85 (2021) 105951

Contents lists available at ScienceDirect

Nano Energy

journal homepage: http://www.elsevier.com/locate/nanoen

# A high performance $CsPbBr_3$ microwire based photodetector boosted by coupling plasmonic and piezo-phototronic effects

Zheng Yang [a,b,1], Mingming Jiang [d,1], Linjuan Guo [b,*], Guofeng Hu [f], Yansong Gu [b], Jianguo Xi [a], Zhihao Huo [a,c], Fangtao Li [a], Shufang Wang [b,*], Caofeng Pan [a,c,e,f,**]

[a] CAS Center for Excellence in Nanoscience, Beijing Key Laboratory of Micro-nano Energy and Sensor, Beijing Institute of Nanoenergy and Nanosystems, Chinese Academy of Sciences, Beijing 100083, China
[b] Hebei Key Laboratory of Optic-Electronic Information and Materials, National & Local Joint Engineering Laboratory of New Energy Photoelectric Devices, College of Physics Science and Technology, Hebei University, Baoding 071002, China
[c] School of Nanoscience and Technology, University of Chinese Academy of Sciences, Beijing 100049, China
[d] College of Science, Nanjing University of Aeronautics and Astronautics, Nanjing 210016, China
[e] Center on Nanoenergy Research, School of Physical Science and Technology, Guangxi University, Nanning, Guangxi 530004, China
[f] College of Optoelectronic Engineering, Shenzhen University, Shenzhen 518060, China

ARTICLE INFO

*Keywords:*
Photodetector
$CsPbBr_3$ microwire
LSPR effect
Piezo-phototronic effect

ABSTRACT

Lead halide perovskites have attracted much attention in photodetector fabrication. Up to now, several strategies have been used to modulate the device performance. Here, P3HT-$CsPbBr_3$ monocrystalline microwires based photodetectors are demonstrated by coupling LSPR and piezo-phototronic effects. The photocurrent, response speed and recovery speed under 532 nm laser illumination were increased to nearly 3.5, 70 and 8.4 times when decorated with Au NCs and applied with a compressive strain of −0.29%, respectively. The enhancement of performances can be attributed to the increased light absorption caused by LSPR effect and the enhanced separation of photo-generated holes at the heterojunction interface caused by piezo-phototronic effect. This work suggests that all-inorganic perovskites $CsPbBr_3$ based photodetectors can be significantly enhanced by coupling plasmonic and piezo-phototronic effects. This strategy can be used to modulate the performance of optoelectronic devices based on other piezoelectric materials.

## 1. Introduction

Photodetectors have comprehensive applications in military and civilian fields such as environmental sensing, missile guidance, optical communications, optical imaging and biological analysis [1–7]. Recently, lead halide perovskites have attracted great attentions in optoelectronics such as solar cells, light emitting diodes and photodetectors [8–14]. Their excellent photoelectric properties such as large absorption coefficient, high carrier mobility, long carrier lifetime and diffusion length, low defect density and tunable direct band gap [15–18] make them ideal candidates for photodetector applications. To develop perovskite based photodetectors with high performance, different techniques such as controlled growth of low dimensional single crystals [19–21], fabrication of heterojunctions [22–24], and optimization of devices structure [25,26] have been used. Recently, localized surface plasmon resonance (LSPR) effect based photodetectors have demonstrated excellent plasmon-enhanced performance due to the enhanced local electric field on the surface of plasmonic nanoparticles (NPs) [27,28]. Plasmonic modulation can also be applied to the perovskite-based photodetectors [29,30]. For example, Li and co-workers constructed a high performance flexible UV photodetector by employing $CsPbCl_3$/Ag/OPCs hybrids [31]. Compared with bare $CsPbCl_3$ photodetector, the performance was significantly enhanced through the plasmon and photonic crystals effects.

In addition, the piezo-phototronic effect is another powerful weapon to boost the performance of devices like light emitting diodes [32],

* Corresponding authors.
** Corresponding author at: CAS Center for Excellence in Nanoscience, Beijing Key Laboratory of Micro-nano Energy and Sensor, Beijing Institute of Nanoenergy and Nanosystems, Chinese Academy of Sciences, Beijing 100083, China.
*E-mail addresses:* guolinjuan@hbu.edu.cn (L. Guo), sfwang@hbu.edu.cn (S. Wang), cfpan@binn.cas.cn (C. Pan).
[1] Zheng Yang and Mingming Jiang contributed equally to this work.

https://doi.org/10.1016/j.nanoen.2021.105951
Received 25 January 2021; Received in revised form 28 February 2021; Accepted 1 March 2021
Available online 3 March 2021

strain sensors [33–35], solar cells [36], photodetectors and pressure mapping sensors [37–39] based on semiconductors with non-centrosymmetric crystal structures, superior to other traditional methods [39]. The piezopotential formed at the junction or Schottky interface can change the localized band structure, thus modulating the photon-generated carriers generation, separation, transport, and recombination processes [40–44]. By utilizing the piezo-phototronic effect, the photocurrent, response and recovery speed of a photodetector based on $CH_3NH_3PbI_3$ single crystal were effectively enhanced [45]. Compared with the hybrid ones, all-inorganic perovskites such as $CsPbBr_3$ have shown much higher stability. Utilizing the piezoelectric properties, $CsPbBr_3$ perovskites have shown potential applications as strain-gated photodetectors [46] and wavelength tunable lasers [47]. Besides, one-dimensional $CsPbBr_3$ can be easily synthesized, which is beneficial for piezoelectric device fabrication. Based on the above analysis, the synergistic effects of LSPR and piezo-phototronic effects should be a promising way to boost the performance of 1D $CsPbBr_3$ based photodetectors.

Here, a photodetector with high performance based on single $CsPbBr_3$ monocrystalline microwire (MW) is demonstrated by coupling plasmonic and piezo-phototronic effects. First, 10 nm $SiO_2$ layer was deposited onto the $CsPbBr_3$ MWs, after which Au nanoparticles (NPs) were decorated. The experimental results proved that the sensitivity and response speed were largely improved via the plasmonic effect of Au NPs, coincident with the theoretical simulations. Then, the influence of piezo-phototronic effect on the performances of photodetectors was investigated by applying different tensile and compressive strains. When illuminated with a 532 nm laser (0.318 mW/cm$^2$), the photocurrent further increased by ~145% with a compressive strain of −0.29%. This enhancement is due to the piezopotential induced adjustment of band alignment at heterojunction interface. Our results suggest that the LSPR and piezo-phototronic coupling effect can be a promising strategy for building optoelectronic devices with high performance.

## 2. Experimental section

### 2.1. Growth of $CsPbBr_3$ MWs

The $CsPbBr_3$ monocrystalline MWs with width of 3 μm and length of 300 μm were grown by a PDMS templated antisolvent growth method [46] with some modifications. Brief, a DMSO solution with equal mole of CsBr and $PbBr_2$ (0.25 M) was prepared via magnetic stirring. Then, $CH_3OH$ was dropwise added into DMSO solution at room temperature under vigorous stirring until yellow precipitates no longer disappeared. Then the solution was stirred overnight at 70 °C and finally cooled to 40 °C. 20 μL as-prepared solution was dripped onto a 2 × 2 cm PEN substrate (thickness: 125 μm) with 200 nm $SiO_2$ layer on it. Then a PDMS template with groove arrays (length: 300 μm; width 20 μm; depth: 80 μm) was covered onto PEN substrate and a mild pressure was applied using a clip. Finally, the growth system was transferred into sealed vessel full of $CH_3OH$ vapors. After 36 h, the $CsPbBr_3$ were obtained.

### 2.2. Device fabrication

Au NPs were prepared following a previously reported solution method. [48] After synthesis centrifugation and washing, Au NPs were dispersed into hexane and the concentration is 1 mg/mL. 10 nm $SiO_2$ was deposited onto $CsPbBr_3$ MWs before Au NPs decoration. Then, the Au NPs on the glass substrate were prepared by the self-assembly method reported elsewhere [31]. With slow evaporating of hexane, Au NPs were deposited directly onto $CsPbBr_3$ MWs. Then, chlorobenzene solution containing P3HT (30 mg/mL) was dropped onto one end of the $CsPbBr_3$ MW and heated at 70 °C to form heterojunction. Then silver paste was used as the electrodes for the P3HT and the free end of MW. Finally, the device was packaged with 1 mm (polydimethylsiloxane) PDMS layer to prevent chemical damage. Since the c-axis directions of MWs were unknown before tests, the response among different devices were different.

### 2.3. Characterization and measurements

The XRD pattern, absorption spectra, and PL spectra were obtained with an X' Pert3 powder X-ray diffractometer, a UV–vis–NIR spectrophotometer (Shimadzu UV3600) and a confocal microprobe Raman spectroscope (HORIBA/LabRAM HR Evolution), respectively. The TEM sample was obtained by FIB (focused ion beam) method. The SEM images and TEM images were obtained with a HITACHI SU8020 FE-SEM and a JEOL JEM-2100Plus HRTEM, respectively. The deflection-voltage curves were measured using an Asylum Research/MFP-3D AFM. For photoelectric tests, a 532 nm diode laser was used as light source. An attenuator and a chopper were connected to change the light intensity and turn on/off the light. All the I-V curves were measured with a Keithley 4200-SCS semiconductor parameter analyzer. The I-t characteristic were measured using a signal generator (Stanford Research DS345) and an electrometer (Stanford Research SR570).

## 3. Results and discussion

The $CsPbBr_3$ monocrystalline MWs were synthesized following our previously reported PDMS templated antisolvent growth method [37] with some modifications, which can be seen in the experimental section. Fig. 1a shows a typical low magnification SEM image (up) and optical image of a single monocrystalline $CsPbBr_3$ MW grown on flexible polyethylene naphthalate (PEN) substrate. The microwire is uniform and straight with good crystallinity. The HRTEM and SAED image of a single $CsPbBr_3$ MW in Fig. 1b indicates that the monocrystalline MW belongs to orthorhombic phase with preferred growth direction parallel to the [010] orientation. To demonstrate the LSPR effect on the performance of photodetectors, we tried to incorporate Au NPs onto the MWs via self-assembly method after the growth of MWs. Au NPs were synthesized according to the method reported elsewhere [38]. The prepared Au NPs show narrow-size distributions (Fig. 1d and S1) with an average diameter of 7.9 nm. Fig. S2 shows the clear lattice fringes of Au NPs, proving the successful synthesis. To suppress the charge and energy transfers between $CsPbBr_3$ MWs and Au NPs, a 10 nm layer of $SiO_2$ was deposited onto MWs through thermal evaporation before Au decoration [29]. Then Au NPs were further self-assembled on the surface of $CsPbBr_3$ MWs. Fig. S3 and S4 show the enlarged part of SEM image of $CsPbBr_3$ MW/Au hybrid and the corresponding EDX elemental mapping showing that the compositional distributions of the four elements (Cs, Pb, Br and Au), respectively, from which one can find that the Au NPs disperse uniformly on the $CsPbBr_3$ MW.

The X-ray diffraction (XRD) patterns (Fig. 1c) of the $CsPbBr_3$ MWs and Au NPs belong to orthorhombic phase (ICSD: 97851) and cubic phase (JCPDS: No.04-0784), respectively. The XRD pattern of $CsPbBr_3$/Au hybrids shows the diffraction peaks of both $CsPbBr_3$ MWs and Au NPs, indicating the successful decoration of Au NPs onto $CsPbBr_3$ MWs. Au NPs were hexagonally packed tightly on the $CsPbBr_3$ MW, beneficial to generating the amplified local electric field. As shown in Fig. 1e, the strong absorption band centered at ~530 nm (black one) caused by LSPR of Au NPs matches well with the absorption spectrum of $CsPbBr_3$ MWs (red one), indicating that Au plasmonic enhancement will be available in $CsPbBr_3$/Au hybrids-based devices. Besides, the absorption spectra of $CsPbBr_3$ with and without Au NPs demonstrate that the absorption waveband dose not change after depositing the Au NPs, while the absorbance is enhanced, indicating the LSPR effect enhanced light absorption.

The PL spectra of a single $CsPbBr_3$ MW before and after Au NPs decoration are shown in Fig. 2a. PL intensity of $CsPbBr_3$ MW was enhanced by a factor of ~2 after incorporating with Au NPs. This enhancement value is much smaller than the perovskite films due to that the influence range of LSPR effect is much smaller than size of $CsPbBr_3$

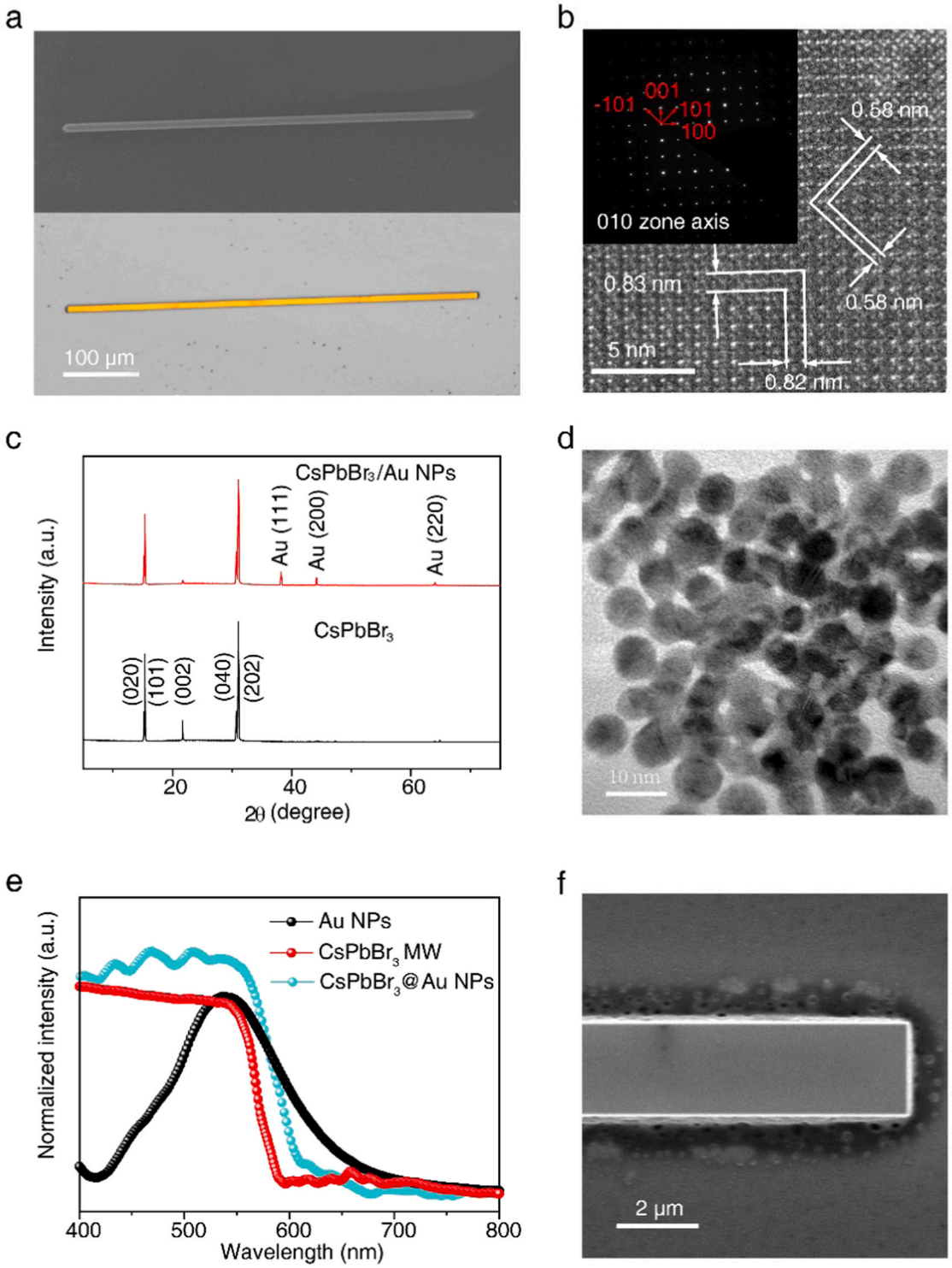


**Fig. 1.** (a) The SEM image (up) and optical image (down) of a single $CsPbBr_3$ MW grown on flexible PEN substrate. (b) High resolution TEM and SAED pattern (inset) showing the [010] zone axis of $CsPbBr_3$ MW. (c) XRD patterns of $CsPbBr_3$ MWs, and $CsPbBr_3$ MWs/Au NPs hybrids. (d) TEM image of monodisperse Au NPs. (e) Absorption spectra of $CsPbBr_3$ MWs (red), Au nanofilm (black) and $CsPbBr_3$ MWs/Au NPs hybrids (f). Magnified SEM image of one end of $CsPbBr_3$ MW/Au NPs hybrid.

MWs. Then, the Finite-Difference Time-Domain (FDTD) simulation was used to calculate the electric field distributions around Au NPs under light illumination. The schematic diagram of simulated device is shown in Fig. S5. A 532 nm incident light is coming along the z-axis and illuminates on the hybrids. Au NPs with a diameter of 8 nm were closely packed on the surface of $CsPbBr_3$ MW wrapping with 10 nm $SiO_2$, and the distance between each NP is 2 nm. Fig. 2b and c demonstrate the field distributions in the xy and xz planes, respectively. The dark red color and dark blue color represent the strongest and weakest local electric field, respectively. A periodic distribution of electric field is generated and the intensity of electric field in the vicinity of Au NPs is significantly enhanced. The simulation results prove that Au LSPR can significantly enhance light absorption and radiation rate of $CsPbBr_3$ MWs. Therefore, the LSPR effect is anticipated to boost the performance

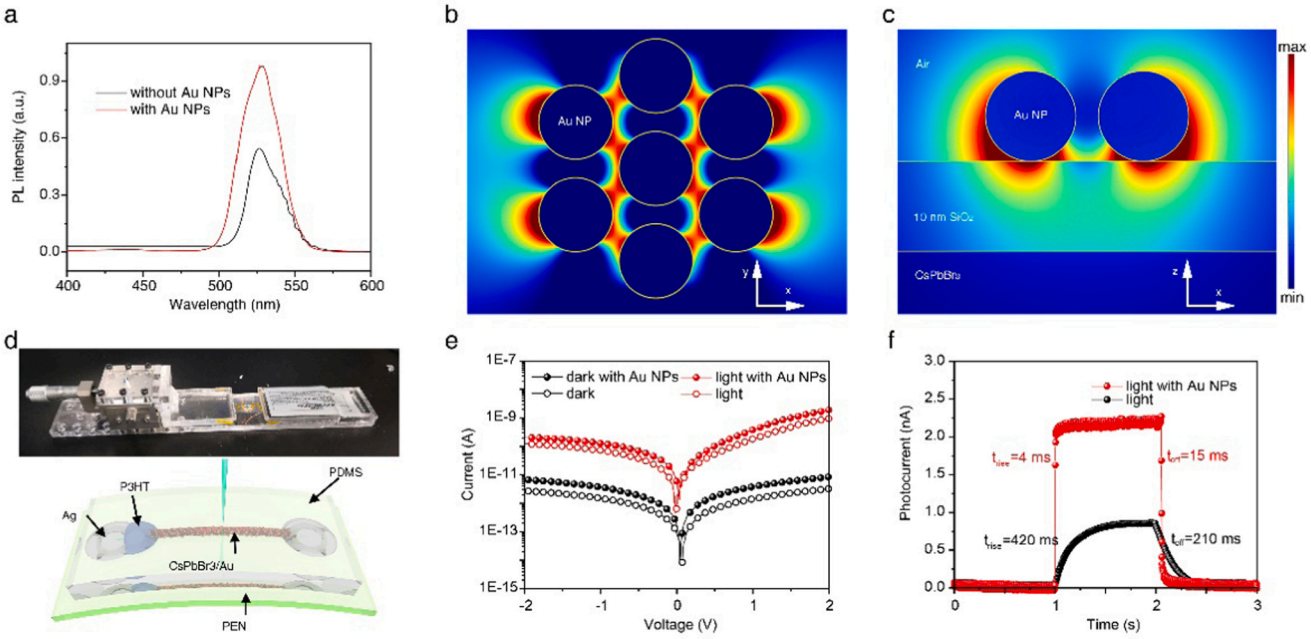


**Fig. 2.** (a) Comparison between PL spectra of a single $CsPbBr_3$ MW before (black) and after (red) Au NPs decoration. FDTD simulations of electric field density distribution at a resonant wavelength of 532 nm in (b) x-y and (c) xz plane. (d) The photograph of the measurement device (up) and schematic diagram (down) of $CsPbBr_3$/Au hybrids-based photodetector. (e) I–V characteristics and (f) I-t characteristic (2 V forward bias) of the P3HT-$CsPbBr_3$ photodetectors with and without Au NPs under 532 nm laser illumination (0.318 mW/cm$^2$).

of $CsPbBr_3$ based photodetectors.

According to our previous report [41], the solution grown $CsPbBr_3$ perovskites show little p-doped conducting behavior. To facilitate studying the piezo-phototronic effect discussed in the following part, a typical p-type semiconductor P3HT with good semiconductivity, stability and a matched band structure with $CsPbBr_3$ was introduced and P3HT-$CsPbBr_3$ MW heterojunction-based photodetectors were fabricated. Fig. 2d shows the photograph experimental setup (up) and schematic diagram (down) of the photodetector. The I-V curve of heterojunction-based device shows a rectifying behavior while the symmetrical linear I-V curve of MW with two Ag electrodes indicates the ohmic contacts (Fig. S6). The fabrication procedure of the photodetectors can be seen in experimental section. Fig. 2e and f show the performance of photodetectors with and without Au NPs under 532 nm illumination. From the I–V curves (Fig. 2e) of the photodetectors with and without Au NPs recorded in dark and under light illumination at 0.318 mW/cm$^2$, one can see that both dark current and photocurrent are enhanced with the decoration of Au NPs. The I-t characteristic in Fig. S6 and Fig. 2f show that at 2 V forward bias, the photocurrent is increased from 0.9 nA to 2.2 nA with an improvement of 2.4 times due to LSPR effect. Fig. S7 shows the photocurrents and dark currents with and without Au NPs at different light intensity. The enhancement factor gradually decreases with the increase of light intensity. Here, enhancement factor is defined as $I_w/I_{wo}$, where $I_w$ and $I_{wo}$ are photocurrents with and without Au NPs at same light intensity, respectively. A comparison of the rise time and fall time of the devices is shown in Fig. S8 with different incident light power. One can see that the rise time and fall time are dramatically shortened. For example, when the light intensity is 0.318 mW/cm$^2$, the rise time and fall time decrease from 420 ms to 6 ms and from 210 ms to 25 ms, respectively (Fig. 2f). The response and recovery speed are 70 and 8.4 times faster than those without Au NPs, respectively. These results may due to that the plasmonic enhanced electric fields make the radiative rate of $CsPbBr_3$ MWs much higher.

The above results prove that Au LSPR can significantly enhance the performance of P3HT-$CsPbBr_3$ MW heterojunction-based photodetectors. Then the performance of the photodetector was tested under light illumination at different light intensity. Fig. 3a shows the typical I-V curves measured in the dark and under 532 nm light illumination with 5 different light intensity ranging from 0.318 mW/cm$^2$ to 6.366 mW/cm$^2$. The asymmetric shape and rectification characteristic of the curves prove the formation of heterojunction. The current at 2 V forward bias increases significantly with the light intensity increasing from 0 to 6.366 mW/cm$^2$ (Fig. 3b). And the rise and fall times at different light intensity can be seen in Fig. S9 with all the rise times less than 8 ms and fall times less than 20 ms. The photocurrents, responsivities and current on/off ratios of the photodetector as a function of intensity are illustrated in Fig. 3c, d. The responsivity is defined as $R = \frac{I_{light}-I_{dark}}{P\times S}$, where P is the illumination light intensity, and S is the effective illuminated area. In this article, the effective illuminated area is measured to be $9.5 \times 10^{-7}$ cm$^2$. One can see clearly that there is a nearly linear relationship between photocurrent ($I_{light}$–$I_{dark}$) and light intensity. While with the increase of light intensity, the responsivity gradually decreases. The responsivity at 0.318 mW/cm$^2$ is ~4.2 A/W. The on/off current ratio is as high as 2400 under illumination of 6.366 mW/cm$^2$. As another two parameters to characterize the performance of a photodetector, external quantum efficiency (EQE) and specific detectivity (D*) are also calculated according to $EQE = \frac{R_\lambda hc}{e\lambda}$ and $D^* = \frac{R_\lambda}{\sqrt{\frac{2eI_d}{S}}}$, where $R_\lambda$ is the responsivity, λ is the light wavelength, $I_d$ is dark current. Here the $I_d$ is about 0.07 nA (Fig. S10). The comparison of the responsivity and EQE of photodetector as a function of wavelength with and without Au NPs is shown in Fig. S11. Both $R_\lambda$ and EQE of the photodetector is greatly enhanced via LSPR effect and the maximum EQE is 11.5%. From Fig. S12 we can find that the maximum D* is $9.9 \times 10^8$ jones. In addition to forward bias, as shown in Fig. S13, the performances of photodetector at a 2 V reverse bias were also evaluated, with the largest responsivity of 0.8 A/W. Fig. S14 shows the stability of photocurrent and dark current versus time. After 1000 times light on-off cycles, both the photocurrent and dark current remain stable with no obviously deterioration and fluctuation, indicating that the photodetectors have good stability.

Then, the piezo-phototronic effect on photodetector performance was investigated by applying different tensile and compressive strains under 532 nm laser illumination. The strains were applied by bending

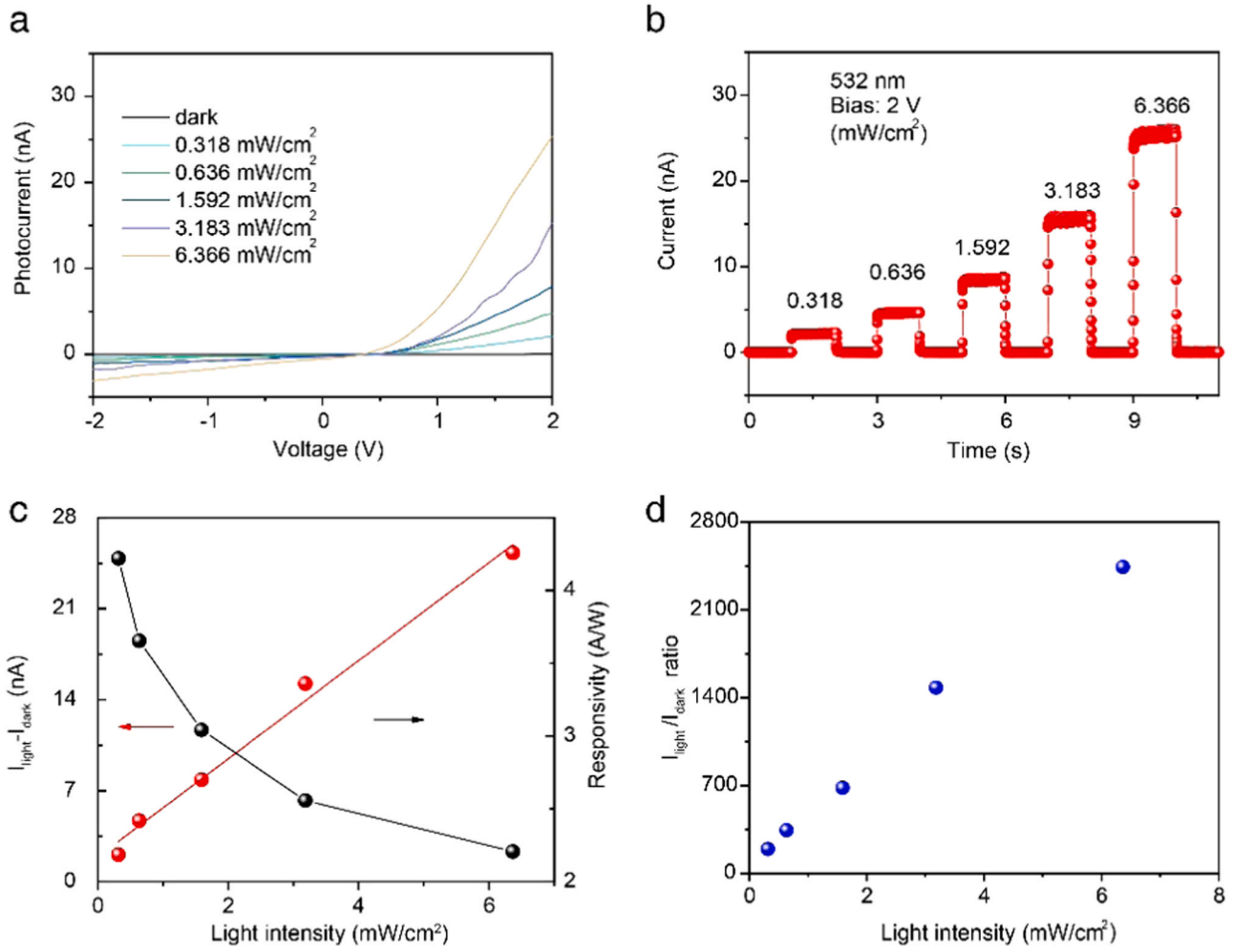


**Fig. 3.** (a) I-V curves of the photodetector under 532 nm light illumination with different intensities. (b) I-t characteristic, (c) photocurrent (red), responsivity (black) and (d) on/off ratio the photodetector under 532 nm light illumination at different light intensity and 2 V forward bias.

the PEN substrates using the manual moving stage shown in Fig. 2d. Since the MWs are fixed onto the substrate, bending of the substrate will lead to the deformation of MWs. Since the length of MW is much smaller than the substrate size, the deformation of MWs can be seen as uniform. The strains can be changed by bending into different angles and calculated according to the our early reports [46]. Since the piezopotential is related to the c-axis ([010] crystal orientation) direction of the $CsPbBr_3$ MWs, two different devices with opposite c-axis directions were fabricated. Fig. 4a and b show the I-V curves of the device with [010] direction pointing to P3HT with three different compressive and tensile strains, respectively (0.318 mW/cm$^2$). It can be clearly seen that the photocurrent at forward bias increases remarkably with the increase of compressive strain (minus sign) while decreases with the increase of tensile strain (positive sign). While at the reverse bias, the photocurrent decreases with the increase of compressive strain while increases with the increase of tensile strains, showing an opposite phenomenon. I-V curves with different strains (6.366 mW/cm$^2$) from − 2 to 2 V are shown in Fig. S15, which demonstrate the same change trend. The asymmetrical results confirm the piezoelectric effect modulation rather than piezoresistive effect on P3HT-$CsPbBr_3$ MW heterojunction-based photodetectors. The photocurrent as a function of strain at different light intensity at forward bias and reverse bias is shown in Fig. 4c and Fig. S16, respectively. The photocurrent increases with the increase of light intensity when the strain keeps the same. For forward bias, when illuminated under laser with same light intensity, the photocurrent gradually decreases with the strain increasing from −0.29–0.31%. For example, when light intensity is 6.366 mW/cm$^2$, photocurrents for strain of −0.29%, 0% and 0.31% are 54, 25.3 and 8.8 nA, respectively. On the contrary, the photocurrent at reverse bias continuously increases when the strain increases from −0.29–0.31%. As shown in Fig. 4d, e and Fig. S17a, b, the responsivity R and its relative change ΔR/R were calculated and plotted as a function of strain, where $\Delta R = R_{strain} - R_0$ ($R_{strain}$ and $R_0$ are responsivities at same light intensity with and without strains). The relation between responsivity and strain shows a similar trend with the photocurrent. With a compressive strain of −0.29% (0.318 mW/cm$^2$), the maximum ΔR/R is about 145%. When the tensile strain is 0.31%, ΔR/R is as low as −64.7% (0.636 mW/cm$^2$). To avoid breakage of $CsPbBr_3$ MWs, tests with stronger strains were not done. The ΔR/R at a −2 V reverse bias were also calculated and shown in Fig. S18. The maximum value of ΔR/R for reverse bias is 91% when tensile strain is 0.31%. Fig. 4f depicts the transient response of the photodetector with different strains. It is worth noting that the response and recovery speeds almost have no change with and without strains. When the c-axis direction of MW is reversed, the experimental phenomena are quite different. As shown in Fig. S19, when applied with tensile strains, the photocurrent at forward bias increases, compared with no strain case. While for compressive conditions, the photocurrent decreases. The piezo-phototropic effect induced modulation of photodetectors' performance is also repeatable and stable. During our 50 cycles' tests, for each bending cycle, once the bending angle is decided, the photocurrent fluctuation is less than 5%. Once the strain is vanished, the photocurrent can always return to the initial value.

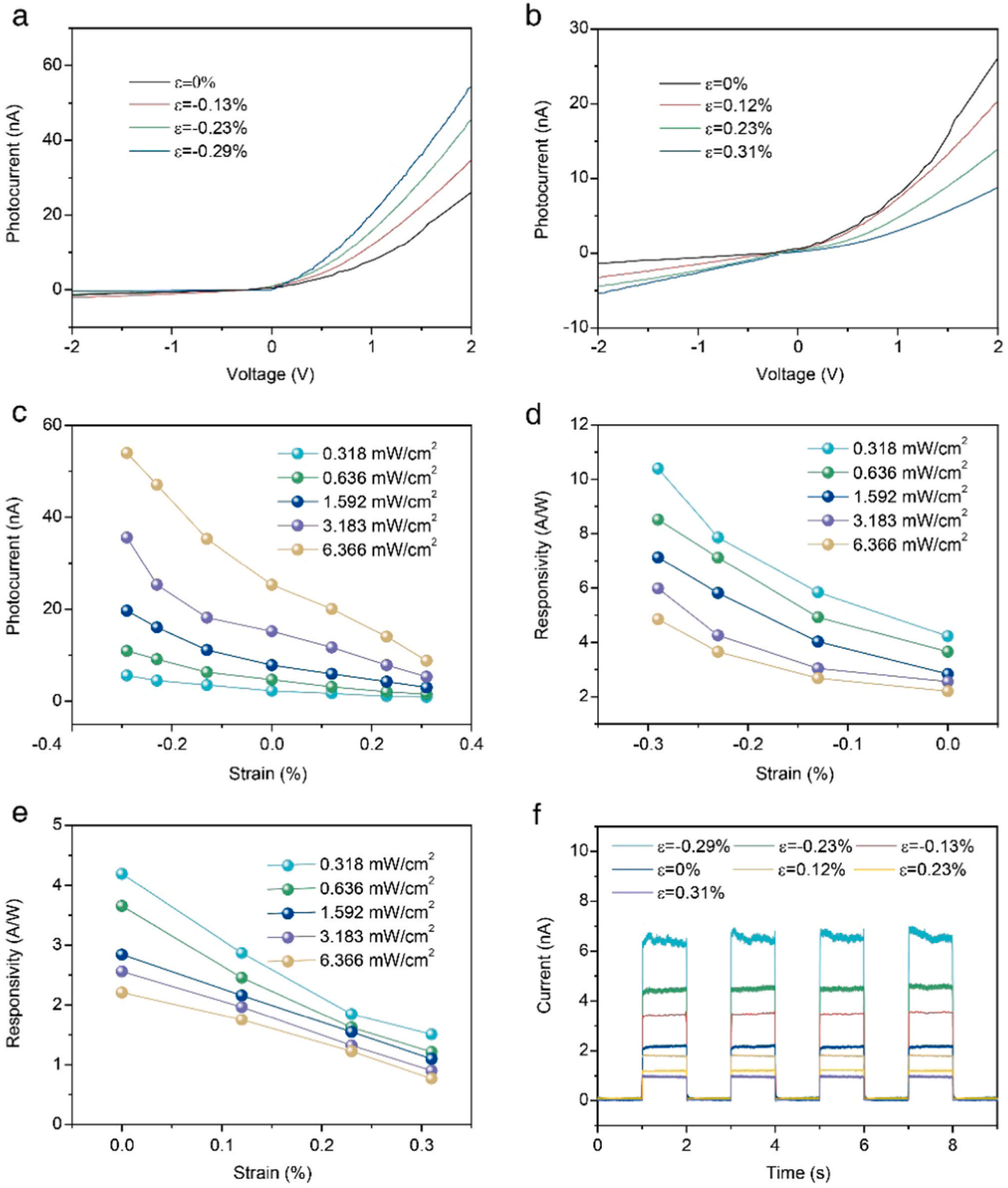


**Fig. 4.** The performance of photodetector with the [010] direction of $CsPbBr_3$ microwire points to P3HT modulated by the piezo-phototronic effect. I–V characteristics of the device with different (a) compressive strains and (b) tensile strains (0.318 mW/cm$^2$). (c) Relationship between the photocurrent and strain at different light intensity and 2 V forward bias. The responsivity as a function of (d) compressive and (e) tensile strain at different light intensity and 2 V forward bias. f) I–t curves of the photodetector under 7 different strains at 2 V forward bias with 0.316 mW/cm$^2$ light intensity.

In order to explore the piezoelectric effect of $CsPbBr_3$, piezoelectric coefficient d33 were first measured. As a 1D material, it is hard to directly measure the d33 of the $CsPbBr_3$ MWs in [010] direction (c-axis). Therefore, $CsPbBr_3$ microplates with normal direction of [010] crystal orientation (Fig. S20) which is equivalent to the c-axis of $CsPbBr_3$ MWs were synthesized according to our previously published literature [49]. As shown in Fig. 5a, the deflection-voltage characteristics of a $CsPbBr_3$ microplate showing a butterfly shape were obtained via piezoresponse force microscopy (PFM) and an average d33 value of 4.56 pm/V was derived from five different curves, which is larger than that of $CsPbBr_3$

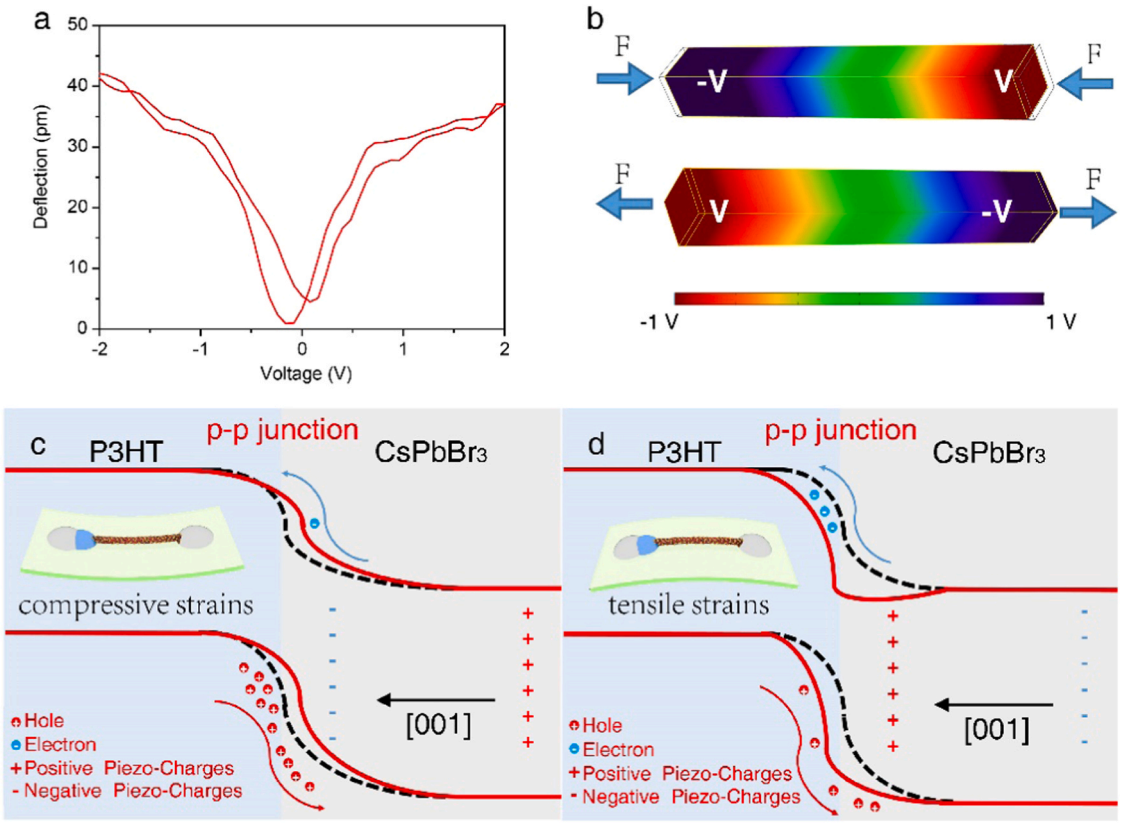


**Fig. 5.** (a) Deflection-voltage characteristics of the $CsPbBr_3$ monocrystalline microplate shown in Fig. S15. (b) COMSOL simulation result piezopotential distribution in the $CsPbBr_3$ MW with different strains. Schematic energy band diagram of the device when applied with (c) compressive strains and (d) tensile strains.

polycrystalline films [50]. To determine the mechanism of the piezo-phototronic effect modulated photodetector performance, the energy band diagrams at the heterojunction interface with no strain, compressive strain and tensile strain were carefully analyzed. The valence bands and conduction bands versus vacuum of the $CsPbBr_3$ are obtained from the literature [51] while the fermi level is calculated from UPS spectrum in Fig. S21. The fermi level of 5.12 eV is closer to valence band, proving a little p-type conducting behavior. Fig. S22 shows the energy band diagram of the p-p heterojunction without strains, in which the [010] direction of $CsPbBr_3$ microwire points to P3HT. When 532 nm laser illuminates on the $CsPbBr_3$, the photocurrent will be generated. By the finite element method, we calculated a piezopotential distribution in a typical $CsPbBr_3$ microwire (Fig. 5b), which can be seen that inverse potential drops will be induced along the length of the MW when applied with tensile strain and compressive trains. When compressive strain is applied, a negative piezopotential is created at the interface, which will attract the holes in P3HT and $CsPbBr_3$ moving toward the heterojunction interface (Fig. 5c). Thus, the localized energy band is shifted up, which will be beneficial for hole transport. When forward bias is applied, the confinement of photo-generated holes produced at $CsPbBr_3$ is effectively weaken, resulting in the photocurrent increase. When at reverse bias, the upward energy band bending will lead to the decrease of built-in field, decreasing separation efficiency of photo-generated electron-hole pairs. Thus, the reverse photocurrent is decreased. On the contrary, as shown in Fig. 5d, when tensile strain is applied, a positive piezopotential is created at the interface, repelling the holes in P3HT and $CsPbBr_3$, leading to the lowered localized energy band. When forward bias is applied, the confinement of photo-generated holes produced at $CsPbBr_3$ is effectively enhanced, resulting in the photocurrent decrease. When at reverse bias, the downward energy band bending will lead to the strengthening of built-in field, increasing separation efficiency and decreasing the reverse photocurrent. When the [010] direction of microwire is away from P3HT, compressive strains will lead to the creation of positive piezopotential and tensile strains will lead to the creation of negative piezopotential, resulting in the opposite photocurrent change trend.

## 4. Conclusion

In conclusion, P3HT-$CsPbBr_3$ MW heterojunction-based photodetectors were fabricated and plasmonic and piezo-phototronic coupling effects were used to boost the performance of photodetectors. First, Au NPs whose plasmonic peak matching with absorption wavelength of $CsPbBr_3$ were synthesized and decorated onto $CsPbBr_3$. Field enhancement was confirmed by FDTD simulation. P3HT-$CsPbBr_3$ MW heterojunction was fabricated using a standard solution method. After introducing LSPR effect, the photocurrent, response speed and recovery speed were significantly enhanced 2.4, 70 and 8.4 times, respectively. Then, the photocurrents were further modulated by applying different and compressive tensile strains, exhibiting an obvious responsivity improvement of 145% (0.318 mW/cm$^2$, 2 V bias, −0.29% compressive strain), due to the change of energy band at heterojunction interface induced by piezopotential. A piezoelectric coefficient of 4.56 pm/V of the $CsPbBr_3$ single crystal in [010] direction was also obtained via PFM measurement. These results prove that coupling plasmonic and piezo-phototronic effect is an effective strategy to boost the performance of $CsPbBr_3$ photodetectors, and it can be used in other lead halide perovskite-based optoelectronics devices.

## CRediT authorship contribution statement

**Zheng Yang:** Writing - original draft preparation, Writing - review & editing, Investigation, Formal analysis, Methodology, Software. **Mingming Jiang:** Simulation, Investigation, Methodology, Software.

**Linjuan Guo:** Investigation, Methodology, Software. **Guofeng Hu:** Investigation, Methodology. **Yansong Gu:** Methodology, Software. **Jianguo Xi:** Investigation. **Zhihao Huo:** Investigation. **Fangtao Li:** Investigation. **Shufang Wang:** Resources, Validation, Funding acquisition. **Caofeng Pan:** Project administration, MS writing and revising, Investigation, Formal analysis, Resources, Supervision, Validation, Funding acquisition.

## Declaration of Competing Interest

The authors declare that they have no known competing financial interests or personal relationships that could have appeared to influence the work reported in this paper.

## Acknowledgements

The authors thank the support of National Key Research and Development Project from Minister of Science and Technology, China (2016YFA0202703), National Natural Science Foundation of China (No. 61675027, 51622205, 51432005, 61805015, 61804011 and 51972094), Beijing City Committee of Science and Technology (Z171100002017019 and Z181100004418004), Beijing Natural Science Foundation (4181004, 4182080, 4184110, 2184131 and Z180011), Shenzhen Science and Technology Program (Grant No. KQTD20170810105439418), the Nature Science Foundation of Hebei Province (E2020201025) and the Advanced Talents Incubation Program of the Hebei University (521000981351 and 521000981287).

## Appendix A. Supporting information

Supplementary data associated with this article can be found in the online version at doi:10.1016/j.nanoen.2021.105951.

## References

[1] S. Cai, X. Xu, W. Yang, J. Chen, X. Fang, Materials and designs for wearable photodetectors, Adv. Mater. 31 (2019), 1808138.
[2] P.C.Y. Chow, T. Someya, Adv. Mater. (2019), 1902045.
[3] N. Huo, G. Konstantatos, Recent progress and future prospects of 2D-based photodetectors, Adv. Mater. 30 (2018), 1801164.
[4] T. Lin, J. Wang, Strategies toward high-performance solution-processed lateral photodetectors, Adv. Mater. 31 (2019), 1901473.
[5] Y. Gao, X. Gong, W. Fang, A. Ishida, Growth and characteristics of InAsSb epilayers with a cutoff wavelength of 4.8 μm prepared by one-step liquid phase epitaxy, Rare Met. 28 (2009) 313–316.
[6] B. He, Y.-X. Ren, T.-J. Dai, S. Hou, X.-Z. Liu, Characterization and performance ofgraphene–PbSe thin film heterojunction, Rare Met. 40 (2021) 1–6.
[7] H.-Y. Yin, H. Cai, R.-S. Cheng, Z. Xu, Z.-N. Jiang, J.-S. Liu, T.-F. Li, W. Chen, Polarization independent superconducting nanowire detector with high-detection efficiency, Rare Met. 34 (2015) 71–76.
[8] M.V. Kovalenko, L. Protesescu, M.I. Bodnarchuk, Properties and potential optoelectronic applications of lead halide perovskite nanocrystals, Science 358 (2017) 745–750.
[9] H. Tsai, R. Asadpour, J.-C. Blancon, C.C. Stoumpos, O. Durand, J.W. Strzalka, B. Chen, R. Verduzco, P.M. Ajayan, S. Tretiak, J. Even, M.A. Alam, M.G. Kanatzidis, W. Nie, A.D. Mohite, Light-induced lattice expansion leads to high-efficiency perovskite solar cells, Science 360 (2018) 67–70.
[10] W.S. Yang, B.-W. Park, E.H. Jung, N.J. Jeon, Y.C. Kim, D.U. Lee, S.S. Shin, J. Seo, E. K. Kim, J.H. Noh, S.I. Seok, Iodide management in formamidinium-lead-halide–based perovskite layers for efficient solar cells, Science 356 (2017) 1376–1379.
[11] K. Lin, J. Xing, L.N. Quan, F.P.G. de Arquer, X. Gong, J. Lu, L. Xie, W. Zhao, D. Zhang, C. Yan, W. Li, X. Liu, Y. Lu, J. Kirman, E.H. Sargent, Q. Xiong, Z. Wei, Perovskite light-emitting diodes with external quantum efficiency exceeding 20 per cent, Nature 562 (2018) 245–248.
[12] J. Chen, W. Du, J. Shi, M. Li, Y. Wang, Q. Zhang, X. Liu, Perovskite quantum dot lasers, InfoMat 2 (2020) 170–183.
[13] P. Lu, M. Lu, H. Wang, N. Sui, Z. Shi, W.W. Yu, Y. Zhang, Metal halide perovskite nanocrystals and their applications in optoelectronic devices, InfoMat 1 (2019) 430–459.
[14] Ying Li, Zhi-Feng Shi, Xin-Jian Li, Chong-Xin Shan, Photodetectors based on inorganic halide perovskites: materials and devices, Chin. Phys. B 28 (2019), 017803.
[15] M. Ahmadi, T. Wu, B. Hu, A review on organic-inorganic halide perovskite photodetectors: device engineering and fundamental physics, Adv. Mater. 29 (2017), 1605242.
[16] K. Leng, I. Abdelwahab, I. Verzhbitskiy, M. Telychko, L. Chu, W. Fu, X. Chi, N. Guo, Z. Chen, Z. Chen, C. Zhang, Q.-H. Xu, J. Lu, M. Chhowalla, G. Eda, K.P. Loh, Molecularly thin two-dimensional hybrid perovskites with tunable optoelectronic properties due to reversible surface relaxation, Nat. Mater. 17 (2018) 908–914.
[17] S.-F. Leung, K.-T. Ho, P.-K. Kung, V.K.S. Hsiao, H.N. Alshareef, Z.L. Wang, J.-H. He, A self-powered and flexible organometallic halide perovskite photodetector with very high detectivity, Adv. Mater. 30 (2018), 1704611.
[18] Y. Wang, R. Fullon, M. Acerce, C.E. Petoukhoff, J. Yang, C. Chen, S. Du, S.K. Lai, S. P. Lau, D. Voiry, D. O'Carroll, G. Gupta, A.D. Mohite, S. Zhang, H. Zhou, M. Chhowalla, Solution-processed $MoS_2$/organolead trihalide perovskite photodetectors, Adv. Mater. 29 (2017), 1603995.
[19] J. Feng, C. Gong, H. Gao, W. Wen, Y. Gong, X. Jiang, B. Zhang, Y. Wu, Y. Wu, H. Fu, L. Jiang, X. Zhang, Single-crystalline layered metal-halide perovskite nanowires for ultrasensitive photodetectors, Nat. Electron. 1 (2018) 404–410.
[20] Y. Zhao, Y. Qiu, H. Gao, J. Feng, G. Chen, L. Jiang, Y. Wu, Layered-perovskite nanowires with long-range orientational order for ultrasensitive photodetectors, Adv. Mater. 32 (2020), 1905298.
[21] Y. Liu, Y. Zhang, Z. Yang, H. Ye, J. Feng, Z. Xu, X. Zhang, R. Munir, J. Liu, P. Zuo, Q. Li, M. Hu, L. Meng, K. Wang, D.-M. Smilgies, G. Zhao, H. Xu, Z. Yang, A. Amassian, J. Li, K. Zhao, S. Liu, Multi-inch single-crystalline perovskite membrane for high-detectivity flexible photosensors, Nat. Commun. 9 (2018) 5302.
[22] F. Cao, W. Tian, L. Meng, M. Wang, L. Li, Ultrahigh-performance flexible and self-powered photodetectors with ferroelectric P(VDF-TrFE)/perovskite bulk heterojunction, Adv. Funct. Mater. 29 (2019), 1808415.
[23] X. Geng, F. Wang, H. Tian, Q. Feng, H. Zhang, R. Liang, Y. Shen, Z. Ju, G.-Y. Gou, N. Deng, Y.-T. Li, J. Ren, D. Xie, Y. Yang, T.-L. Ren, Ultrafast photodetector by integrating perovskite directly on silicon wafer, ACS Nano 14 (2020) 2860–2868.
[24] M. Wang, W. Tian, F. Cao, M. Wang, L. Li, Flexible and self-powered lateral photodetector based on inorganic perovskite $CsPbI_3$–$CsPbBr_3$ heterojunction nanowire array, Adv. Funct. Mater. 30 (2020), 1909771.
[25] A. Daus, C. Roldan-Carmona, K. Domanski, S. Knobelspies, G. Cantarella, C. Vogt, M. Gratzel, M.K. Nazeeruddin, G. Troster, Metal-Halide perovskites for gate dielectrics in field-effect transistors and photodetectors enabled by PMMA lift-off process, Adv. Mater. 30 (2018), 1707412.
[26] J. Zeng, C. Meng, X. Li, Y. Wu, S. Liu, H. Zhou, H. Wang, H. Zeng, Interfacial-tunneling-effect-enhanced CsPbBr3 photodetectors featuring high detectivity and stability, Adv. Funct. Mater. 29 (2019), 1904461.
[27] J.-A. Huang, L.-B. Luo, Low-dimensional plasmonic photodetectors: recent progress and future opportunities, Adv. Opt. Mater. 6 (2018), 1701282.
[28] A. Zada, P. Muhammad, W. Ahmad, Z. Hussain, S. Ali, M. Khan, Q. Khan, M. Maqbool, Adv. Funct. Mater. (2019), 1906744.
[29] B. Du, W. Yang, Q. Jiang, H. Shan, D. Luo, B. Li, W. Tang, F. Lin, B. Shen, Q. Gong, X. Zhu, R. Zhu, Z. Fang, Plasmonic-functionalized broadband perovskite photodetector, Adv. Opt. Mater. 6 (2018), 1701271.
[30] B. Liu, R.R. Gutha, B. Kattel, M. Alamri, M. Gong, S.M. Sadeghi, W.-L. Chan, J. Z. Wu, Using Silver Nanoparticles-Embedded Silica Metafilms as Substrates to Enhance the Performance of Perovskite Photodetectors, ACS Appl. Mater. Interfaces 11 (2019) 32301–32309.
[31] D. Li, D. Zhou, W. Xu, X. Chen, G. Pan, X. Zhou, N. Ding, H. Song, Plasmonic photonic crystals induced two-order fluorescence enhancement of blue perovskite nanocrystals and its application for high-performance flexible ultraviolet photodetectors, Adv. Funct. Mater. 28 (2018), 1804429.
[32] R. Bao, C. Wang, Z. Peng, C. Ma, L. Dong, C. Pan, Light-emission enhancement in a flexible and size-controllable ZnO nanowire/organic light-emitting diode array by the piezotronic effect, ACS Photonics 4 (2017) 1344–1349.
[33] Y. Peng, J. Lu, D. Peng, W. Ma, F. Li, Q. Chen, X. Wang, J. Sun, H. Liu, C. Pan, Dynamically modulated GaN whispering gallery lasing mode for strain sensor, Adv. Funct. Mater. 29 (2019), 1905051.
[34] C.F. Wang, C.F. Pan, Z.L. Wang, Electronic skin for closed-loop systems, ACS Nano 13 (2019) 12287–12293.
[35] R. Bao, J. Tao, C. Pan, Z.L. Wang, Piezo-phototronic effect in nano-sensors, Small Sci. (2021), 2000060.
[36] S. Qiao, J. Liu, G. Fu, K. Ren, Z. Li, S. Wang, C. Pan, ZnO nanowire based CIGS solar cell and its efficiency enhancement by the piezo-phototronic effect, Nano Energy 49 (2018) 508–514.
[37] R. Bao, C. Wang, L. Dong, R. Yu, K. Zhao, Z.L. Wang, C. Pan, Flexible and controllable piezo-phototronic pressure mapping sensor matrix by ZnO NW/p-polymer LED array, Adv. Funct. Mater. 25 (2015) 2884–2891.
[38] X. Wang, H. Zhang, R. Yu, L. Dong, D. Peng, A. Zhang, Y. Zhang, H. Liu, C. Pan, Z. L. Wang, Dynamic pressure mapping of personalized handwriting by a flexible sensor matrix based on the mechanoluminescence process, Adv. Mater. 27 (2015) 2324–2331.

[39] X. Wang, D. Peng, B. Huang, C. Pan, Z.L. Wang, Piezophotonic effect based on mechanoluminescent materials for advanced flexible optoelectronic applications, Nano Energy 55 (2019) 389–400.
[40] J. Ren, W. Zhang, Y. Wang, Y. Wang, J. Zhou, L. Dai, M. Xu, A graphene rheostat for highly durable and stretchable strain sensor, InfoMat 1 (2019) 396–406.
[41] C. Pan, L. Dong, G. Zhu, S. Niu, R. Yu, Q. Yang, Y. Liu, Z.L. Wang, High-resolution electroluminescent imaging of pressure distribution using a piezoelectric nanowire LED array, Nat. Photonics 7 (2013) 752–758.
[42] Z.L. Wang, Piezopotential gated nanowire devices: piezotronics and piezo-phototronics, Nano Today 5 (2010) 540–552.
[43] Z.L. Wang, Progress in piezotronics and piezo-phototronics, Adv. Mater. 24 (2012) 4632–4646.
[44] L. Zhu, Q. Lai, W. Zhai, B. Chen, Z.L. Wang, Piezo-phototronic effect enhanced polarization-sensitive photodetectors based on cation-mixed organic–inorganic perovskite nanowires, Mater. Today 37 (2020) 56–63, 37.
[45] Q. Lai, L. Zhu, Y. Pang, L. Xu, J. Chen, Z. Ren, J. Luo, L. Wang, L. Chen, K. Han, P. Lin, D. Li, S. Lin, B. Chen, C. Pan, Z.L. Wang, Piezo-phototronic effect enhanced photodetector based on $CH_3NH_3PbI_3$ single crystals, ACS Nano 12 (2018) 10501–10508.
[46] Q. Xu, Z. Yang, D. Peng, J. Xi, P. Lin, Y. Cheng, K. Liu, C. Pan, $WS_2$/$CsPbBr_3$ van der Waals heterostructure planar photodetectors with ultrahigh on/off ratio and piezo-phototronic effect-induced strain-gated characteristics, Nano Energy 65 (2019), 104001.
[47] Z. Yang, J. Lu, M. ZhuGe, Y. Cheng, J. Hu, F. Li, S. Qiao, Y. Zhang, G. Hu, Q. Yang, D. Peng, K. Liu, C. Pan, Controllable growth of aligned monocrystalline $CsPbBr_3$ microwire arrays for piezoelectric-induced dynamic modulation of single-mode lasing, Adv. Mater. 31 (2019), 1900647.
[48] Y. Dong, Y. Gu, Y. Zou, J. Song, L. Xu, J. Li, F. Xue, X. Li, H. Zeng, Improving all-inorganic perovskite photodetectors by preferred orientation and plasmonic effect, Small 12 (2016) 5622–5632.
[49] Z. Yang, Q. Xu, X. Wang, J. Lu, H. Wang, F. Li, L. Zhang, G. Hu, C. Pan, Large and ultrastable all-inorganic $CsPbBr_3$ monocrystalline films: low-temperature growth and application for high-performance photodetectors, Adv. Mater. 30 (2018), 1802110.
[50] P.A. Dement'ev, M.S. Dunaevskii, L.B. Matyushkin, A.V. Nezhdanov, A.N. Smirnov, D.O. Filatov, Study of $CsPbBr_3$ nanocrystals and their agglomerates by combined scanning probe microscopy and optical spectrometry, Opt. Spectrosc. 125 (2018) 858–863.
[51] Sjoerd A. Veldhuis, Pablo P. Boix, Natalia Yantara, Mingjie Li, Tze Chien Sum, Nripan Mathews, Subodh G. Mhaisalkar, Perovskite materials for light-emitting diodes and lasers, Adv. Mater. 28 (2016) 6804–6834.

**Dr. Zheng Yang** received his PhD degree in Nanoscience and Nanotechnology from the Beijing Institute of Nanoenergy and Nanosystems (CAS) in 2019. Then he joined the College of Physics Science and Technology at Hebei University. His research is mainly focused on the controllable growth and optoelectronics applications of lead halide perovskites.

**Dr. Mingming Jiang** is currently a professor in College of Science, Nanjing University of Aeronautics and Astronautics. His main research interests focus on the fields of low- dimensional semiconductor optoelectronic materials and devices.

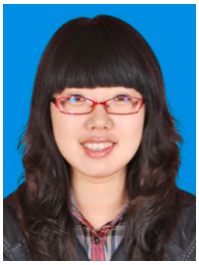

**Dr. Linjuan Guo** obtained her PhD in Xinjiang Technical Institute of Physics & Chemistry, CAS in 2017. Then she joined the College of Physics Science and Technology at Hebei University in 2019. Her research interest is mainly focused on design, preparation and optoelectronics applications of 2D perovskites.

**Dr. Guofeng Hu** received his undergraduate degree from Tianjin Polytechnic University in 2010. Then, he received his PhD from Beijing Institute of Nanoenergy and Nanosystems, CAS under the supervision of Prof. Caofeng Pan in 2015. Currently, he is a post-doctoral researcher at Shenzhen University. His research is mainly focused on photoelectric devices and electronic applications of piezotronics and piezophototronics based on 2D materials.

**Yansong Gu** obtained his bachelor's degree in physics from Baoding College in Baoding, Hebei Province in 2019. He entered into Hebei University to study for a master's degree in 2019. His research interests are controlled growth of lead-halogen perovskite low-dimensional single crystals and plasmonic effect enhanced perovskite photodetectors.

**Dr. Jianguo Xi** received his B. S. Degree (2010) in Materials Science and Engineering from Taiyuan University of Science and Technology, and then graduated from China University of Geosciences as a Ph. D. (2015). He then joined Department of Materials Engineering in Auburn University as a postdoctoral fellow. He is currently a joint postdoctor of Dr. Wenjie Mai's group at Jinan University and Dr. Canfeng Pan's group at Beijing Institute of Nanoenergy and Nanosystem, China Academy of Sciences since 2019. His main research interests focus on the fields of 2D materials for fabricating novel Van Der Waals heterostructures and the application in the piezoelectric and piezophototronic devices.

**Zhihao Huo** received his undergraduate degree from the University of Jinan in 2016. Currently he is pursuing his PhD under the supervision of Prof. Caofeng Pan at Beijing Institute of Nanoenergy and Nanosystems, Chinese Academy of Sciences. His current research interests focus on low-dimensional piezoelectric semiconductor micro/nanophotoelectric function device.

**Fangtao Li** is currently a Ph.D. candidate at School of Mathematics and Physics, University of Science and Technology Beijing. He has joined in the group of Professor Caofeng Pan at Beijing Institute of Nanoenergy and Nanosystems, Chinese Academy of Sciences as a visiting student since 2015. His research interests mainly focus on the synthesis of organic-inorganic hybrid perovskite and their application in photoelectric devices.

**Dr. Shufang Wang** received her Ph.D. degree in Optics from the Institute of Physics, Chinese Academy of Sciences in 2004. She then joined in the group of Professor D. Rémiens at IEMN-CNRS, France as a postdoctral fellow and after that joined in the group of Professor Xiaoxing Xi at the Penn. State University as a postdoctral fellow. She is currently a full professor and a group leader at Hebei University of China. Her researches focus on the fields of photoelectric/thermalelectric materials and devices.

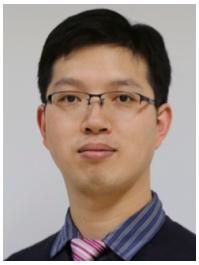

**Dr. Caofeng Pan** received his B.S. degree (2005) and his Ph.D. (2010) in Materials Science and Engineering from Tsinghua University, China. He then joined the Georgia Institute of Technology as a postdoctoral fellow. He is currently a professor and a group leader at Beijing Institute of Nanoenergy and Nanosystems, Chinese Academy of Sciences since 2013. His main research interests focus on the fields of piezotronics/piezo-phototronics for fabricating new electronic and opto-electronic devices, nano-power source (such as nanofuel cell, nano biofuel cell and nanogenerator), hybrid nanogenerators, and self-powered nanosystems. Details can be found at http://piezotronics.binncas.cn/index%20en.php.